RP Current Trends In Applied Sciences
Vol. 1, No. 1 (October – December 2022) pp. 21–25
e-ISSN: 2583-7486

RESEARCH PLATEAU PUBLISHERS

Cite this article: G. Saini, P. Kumari, B.S. Sharma, Examination of nano-crystalline zinc oxide and zinc oxide doped with aluminum using micro-Raman technology, *RP Cur. Tr. Appl. Sci*. **1** (2022) 21–25.

Original Research Article

Examination of nano-crystalline zinc oxide and zinc oxide doped with aluminum using micro-Raman technology

Gopal Saini*, Pinki Kumari, B.S. Sharma
Department of Physics, Lords University, Chikani, Alwar – 301028, Rajasthan, India
*Corresponding author, E-mail: gopal.lordsuniv@gmail.com

ARTICLE HISTORY
Received: 17 Oct. 2022
Revised: 12 Dec. 2022
Accepted: 14 Dec. 2022
Published online: 16 Dec. 2022

KEYWORDS
Raman spectra; nano crystalline ZnO thin films; FTIR spectra.

ABSTRACT
This research uses micro-Raman technology to examine nano-crystalline zinc oxide and zinc oxide doped with aluminium. The substrates were borosilicate glass slides that had been treated with chromic acid and then extensively cleaned in an ultrasonic bath. These substrates were used to deposit both pure and aluminium doped zinc oxide thin films by the dip dry and vacuum evaporation procedures. The X-ray diffraction patterns of all samples with low crystallinity in the films were documented. The estimated d-values from these spectra were compared to the JCPDS powder diffraction file No. 4-831, which represents metallic zinc with a hexagonal closed packed structure. The six Raman-active modes reported at 102, 379, 410, 439, 574 and 591cm^{-1}, correspond to $E^1{}_2$ (low), A_1(TO), E_1(TO), $E^2{}_2$ (high), A_1(LO) and E_1(LO) respectively.

1. Introduction

Understanding the thermoelectrical and optoelectrical capacities requires a detailed understanding of the vibration modes in a single crystal, bulk material, and thin films. The bulk material, which has a uni-axial crystal structure and an optic axis that matches the crystal's c-axis, crystallises as wurtzite, a member of the C^4_{6v} space group. This anisotropy may cause the confined optical phonons and interface phonon's mode in Wurtzite quantum dots to be different from those in zinc blende structures' (isotropic) quantum dots. Additionally, the bulk phonon frequencies of zinc oxide (ZnO) nanostructures' Raman spectra are typically shifted [1-3].

The presence of phonon modes on the higher frequency side is shown by the strong connections between light O atoms and zinc oxide (ZnO), and they prohibit the observation of higher frequency modes linked to even lighter impurity atoms. Numerous investigations have connected the local vibration modes to contaminants, dopants, and defect complexes [4-6]. The behaviour of these peaks and their relationship to quantum dot diameter, however, are debatable. The current work compares these phonon bands in ZnO (powder) and thin films to shed light on the reason behind the shift, broadening, and relative intensities of the peaks.

2. Experimental

Slides made of borosilicate glass that had been cleansed with chromic acid and subsequently cleaned in an ultrasonic bath used as the substrates for the deposition of intrinsic as well as Al doped zinc oxide thin layers using the two processes described below.

(i) Dip Dry: By alternately dipping in a hot water bath maintained at 90^{o}C and a Na_2ZnO_2 bath (0.05 M), thin coatings were deposited over plane glass slides. NaOH and $Zn(NO_3)_2$ were the first precursors. At every time, the substrate was left inside the bath for 40 second after being dipped in the bath 20 times total.

(ii) Vacuum evaporation: In the molybdenum boat, ZnO powder was added in a measured quantity. The substrates were positioned 10 cm above the boat. For the calculated amount of Al doping, ZnO powder and Al powder were combined and thoroughly homogenised. A vacuum of the order of 1.33×10^{-4} Pa was drawn into the reaction chamber after it was shut. By running an electric current through the Molybdenum boat, the powder sample was vapourized for 5 seconds, and then thin films were produced on the glass substrate. These films underwent a 2-hour annealing process in a furnace operating at ambient pressure and 350^{o}C (± 5^{o}C). Using an X-ray's powder spectrometer fitted with a PW1830 X-ray producer for phase determination, all films that were deposited using the aforementioned methods were examined. InVia Renishaw's micro-Raman spectrometer with tangential spectrum resolution, a maximum Raman shifting of 0.8 cm^{-1}, confocal resolution ~ 2.2 micro-meter, and horizontal-vertical resolution ~ 0.2 micro-meter was used to capture the non-resonant Raman spectra in wave number regime from 10 cm^{-1} to 3200 cm^{-1}. An Ar-ion laser source's 514 nm line was employed for excitation, with an incident laser power of 20 mW. The grating utilised in the optical regime had 2000/mm of lines. At room temperature (≈ 27^{o}C), all the spectrum was recorded on back-scattered setup.

3. Results and discussion

Dip Dry: Figure 1 depicts XRD plots of dip-and-dry-prepared doped and undoped thin films. The polycrystalline structure of the thin films is indicated by clearly defined

reflections in the XRD patterns. The structure is wurtzite-arranged and hexagonal in shape. Two additional reflections that correlate to the hydroxide phase may be seen on the undoped material (wulfingite, Card no. 38-385). These extra reflections are absent in zinc oxide thin films having a doping of 2.4, 4.8, and 7.0 At. wt.% aluminium (Figure 1: curves b, c, and d), showing that the insertion of Al^{3+} ion in lattice suppresses the development of the OH^- phases. All these films retain their crystallinity, and no privileged creation in any direction occurs. But, the intensity in the <002> direction significantly increases in 4.8 At. wt.% aluminium doped zinc oxide thin films. It was found that as the number of dipping and drying processes rose, so did the film's thickness. The lattice strain is reduced for low Al doping concentrations (2.5 at wt%), but it increases along with the thickness for high Al concentrations. However, all of the films' densities rise. Normal point dislocations, oxygen valencies, cataion vacancies, and other point defects cause a change in the lattice constants and other parameters like density, bulk modulus, etc. for thin films with a structure that deviates from an ideal crystal structure. As a result, thin films are thinner at lower concentrations of Al^{3+} and thicker at higher concentrations, even though the size of the crystallites doesn't change. Sharp peaks in doped films are seen by laser Raman tests, which confirms improved long-range order (Figure 2).

Despite the presence of both the stronger and the weaker bands in films, the bands' positions and intensities alter when aluminium is doped at various levels. The spectra's basic characteristics stay the same, but more subtle characteristics such as FWHM, the field amplitude, and the peak positions modify. For instance, the inclusion of the Al^{3+} ion significantly reduces the small signal band's strength at 145 cm^{-1} and causes the peak's position to shift to the higher side. Similar to this, none of films of zinc oxide doped with Al^{3+} ions exhibit any of the low frequency bands, viz. 154 cm^{-1}, 212 cm^{-1}, 244 cm^{-1}, and 259 cm^{-1} that were detected in zinc oxide films. In this instance, the main casualty is the intensity drop of the 366 cm^{-1} and 382 cm^{-1} bands at an illuminance of the 435 cm^{-1} band ($E_2^{(2)}$ high mode). Overall, there are twelve phonon modes in ZnO, six of which are Raman active exclusively and identified by Ashkenov et al. [6]. These are E^1_2 (low) (at 102 cm^{-1}), A_1(TO) (at 379 cm^{-1}), E_1(TO) (at 410 cm^{-1}), E^2_2 (high) (at 439 cm^{-1}), A_1(LO) (at 574 cm^{-1}), and E_1(LO) (at 591 cm^{-1}).

In reality, depending on the dimensions and configuration of the crystallites, the Raman spectra for transition metal oxides found in the published research papers differ from one sample to the other sample. In the context of ZnO nano-crystalline films, it assumes a specific relevance. The Raman-active bands corresponding to LO and TO, are most impacted. Hence, the nano-crystalline structure of film is what causes the Raman bands to shift to larger magnitude of wave numbers. Zn atoms weigh 65.39 a.m.u., which is nearly four times more than oxygen atoms (15.999 a.m.u.). Therefore, it is thought that oscillations from O-atom may be implicated in ZnO Wurtzite geometry. Small signal Raman maxima may be typically attributed to the lattice oscillations. As a result, Raman peaks at 145 cm^{-1} and 154 cm^{-1} may be due to lattice oscillations, whereas the Raman maxima at 212 cm^{-1}, 244 cm^{-1}, and 259 cm^{-1} are the result of the deformation mode, which vanish with addition of the Al^{3+} ions. The $E_2^{(2)}$ Raman mode in ZnO arises at 439 cm^{-1}, and multi-phonon process is assigned to the line at 332 cm^{-1}, which also arises in ZnO films [5]. As a result, the 437 cm^{-1} band that we observed is caused by a nonpolar vibrational mode in thin ZnO:Al films, and this nonpolar dealings intensifies when Al^{3+} is added to ZnO. With the addition of contaminants, the film's quality improves, and this is convincingly demonstrated by XRD and EPM. Despite a substantially lower intensity, the band at 381 cm^{-1} remains the same for zinc oxide thin film and all the doped films. The A_1(TO) mode, that expresses the potency, can be used to explain this band. As a result, there is no discernible distinction between the lattice parameters of doped films and ZnO films. The decrease in the 381 cm^{-1} band, the A_1(TO) mode provides evidence that the introduction of Al^{3+} ions reduces the polar nature of ZnO wurtzite structure.

Vacuum evaporation: All samples' X-ray diffraction patterns reveal the films' weak crystallinity (Figures not shown). The JCPDS file No. 6-822, was matched with the predicted d-values from these spectra. Undoped asdeposited films have crystallite orientation along metallic zinc's three <002>, <100>, and <101> planes. However, orientations along ZnO's <002> and <101> became more prevalent when the films were doped with aluminum by 5.0 At wt%. However, there is no indication of an impurity phase in the diffraction patterns. For Al doping, the crystallinity of the films as-deposited increased. Al doped films were discovered to have lower densities and strains than films that weren't doped with Al.

The metallic films were oxidised to generate ZnO films when the layers were thermally treated in open atmosphere for two hours at 350°C; this process greatly increased the thickness of the films as they were deposited. Films that were not doped increased in thickness by about 14%, but doped films with aluminium increased by an astounding 300%. Due to the dopant atoms' low ionisation energies compared to Zn (899.4 kJ/mol)] and zinc [Al (566.5 kJ/mol), which create bonds with oxygen easily, this may be because the film had a significant amount of oxygen during annealing. The movies showed orientation on the <002> plane. Additionally, as the annealing temperature was raised, all of the maxima in the XRD of annealed samples became sharper (figure not shown). Additionally, the crystallite size increased, showing that the doped films had superior crystallinity than the ZnO film. After annealing, a drop in density was seen, indicating that the lattice was extended to take in atmospheric oxygen atoms. But, the decline in the *c/a* ratio suggests that lattice is expanding less along the *c*-axis than the *a*-axis, which is consistent with Reber's results [7]. Both the samples taken as-deposited and those taken after being annealed revealed that the impurities (Cu, Al, and Sn) had no impact on the crystal structure. In comparison to their as-deposited films, the strain in the crystallites of doped films was also marginally lessened after annealing. The undoped ZnO experienced the greatest reduction in strain after annealing.

The six Raman-active modes at 102 cm^{-1} correspond to E^1_2 (low) mode, 379 cm^{-1} correspond to A_1(TO) mode, 410 cm^{-1} correspond to E_1(TO) mode, 439 cm^{-1} correspond to E^2_2 (high) mode, 574 cm^{-1} correspond to A_1(LO) mode, and 591 cm^{-1} correspond to E_1(LO) mode [6]. While oxygen atoms are linked to the E_2 mode, the E_2 mode is connected to the vibration of heavy zinc sublattice. The peak at 437 cm^{-1} in our measured spectrum for bulk ZnO powder belongs to the E_2

(high) phonon mode, while the peak at 379 cm^{-1} corresponds to the A_1 phonon mode (TO). Between A_1(LO) and E_1, the bulk LO phonon peak arises at 582 cm^{-1} (LO). In contrast, the peak is seen to be faint, as reported by Ashkenov et al. [6]. In the spectra of thin film, the LO phonon peak (582 cm^{-1}) in bulk ZnO powder is not visible. But the thin ZnO sheet has a peak at 553 cm^{-1}. According to Xu et al. [8], the surface phonon mode can be used to explain this peak. The 2nd order Raman processes are said to be responsible for the wide peak at approximately 330 cm^{-1} [5]. The oxygen defect sites are related to the peak at 200 cm^{-1}, which is highly typical of thin films [7].

If the spectra of un-doped ZnO thin film and ZnO bulk powder are examined, it is clear that the thin layer displays various extra in-between peaks. This might be the result of crystallite orientation being random along multiple planes. This leads to a conflict between the short-range inter-atomic force and the long-range electrostatic force, which splits phonon modes and results in complex Raman scattering phenomena. According to Loudon [9], this mixing of A_1 and E_1 modes results in the formation of extra peaks. The E_2 (high) peak in the arsenic-deposited ZnO thin layer has a red shift of approximately 2.7 cm^{-1} from its location in bulk pure powder (437.2 cm^{-1}), which is consistent with the findings of Khan et al. [10]. For this phonon peak shift, a number of explanations have been proposed, including spatial confinement inside dots, phonon localization owing to defects, and generated stretch in the dots because of laser-induced heating. Ritcher et al. [11] examined the space captivity of optical phonon modes and demonstrated that the relaxation of q-vector selection criteria in fixed dimension nano-crystallites causes the Raman spectra of semiconductors to be redshifted and widened. However, Khan et al. [10] demonstrated that the phonon shift caused by spatial confinement within dots and by phonon localization is just a few cm^{-1}, whereas the shift caused by heat-induced strain is much larger. The alterations in band position from 434.5 cm^{-1} in ZnO film to 432.8 cm^{-1}, as seen in our studies for ZnO doped with 5.0 at wt% Cu or Sn, indicate the confinement of phonon within the crystallite. Because of optic-anisotric property of the wurtzite lattice, optical phonons confinement in wurtzite nano crystals results in somewhat distinct variations in Raman spectra. It was demonstrated that the discrete frequency spectrum of the confined phonons differed from that of the bulk phonons. Table 1 lists some additional frequency modes that we have detected in the region of 100 cm^{-1} to 300 cm^{-1}. All of these phonon modes in Cu doped ZnO film were noticed as red-shifted in comparison to the as-deposited undoped ZnO film. Davydov et al. [12] found these new modes in first order Raman spectra and pointed out that these came from areas of a faulty material with a high density of states. When these modes were doped with Sn and Al (5 at wt%), it was discovered that both their frequency and strength decreased.

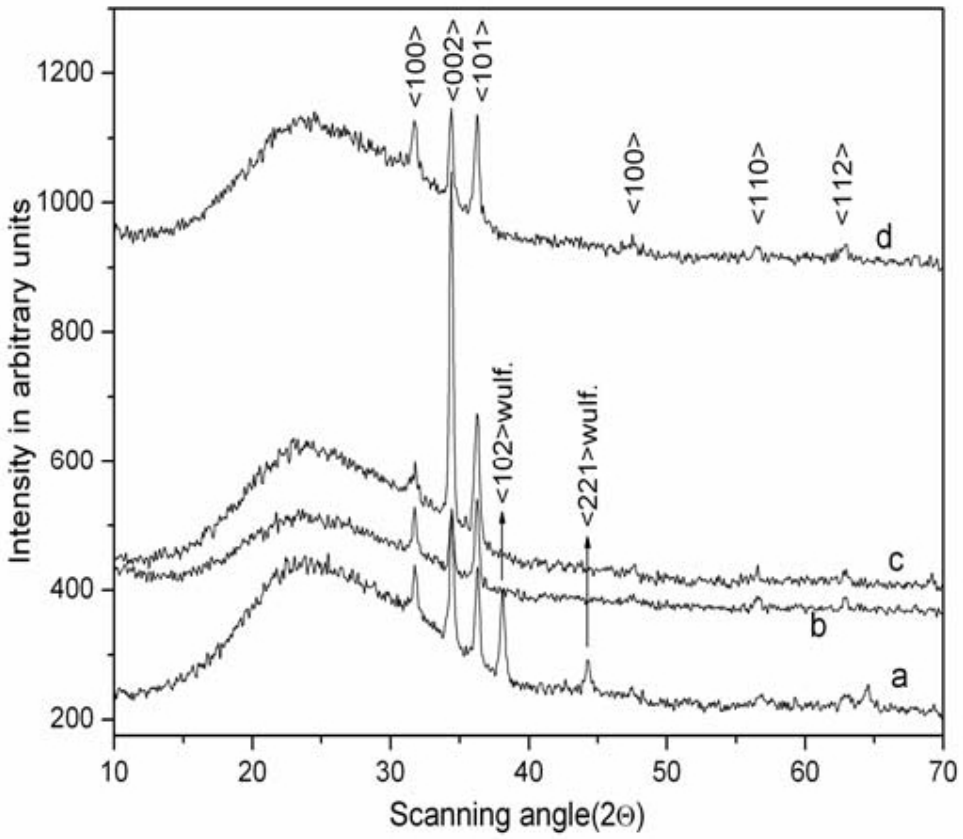

Figure 1. X-ray diffraction pattern of zinc oxide thin films. Here, curves a, b, c, and d stand for un-doped zinc oxide and 2.5, 5.0and 7.5 at. wt % aluminum doped zinc oxide, respectively.

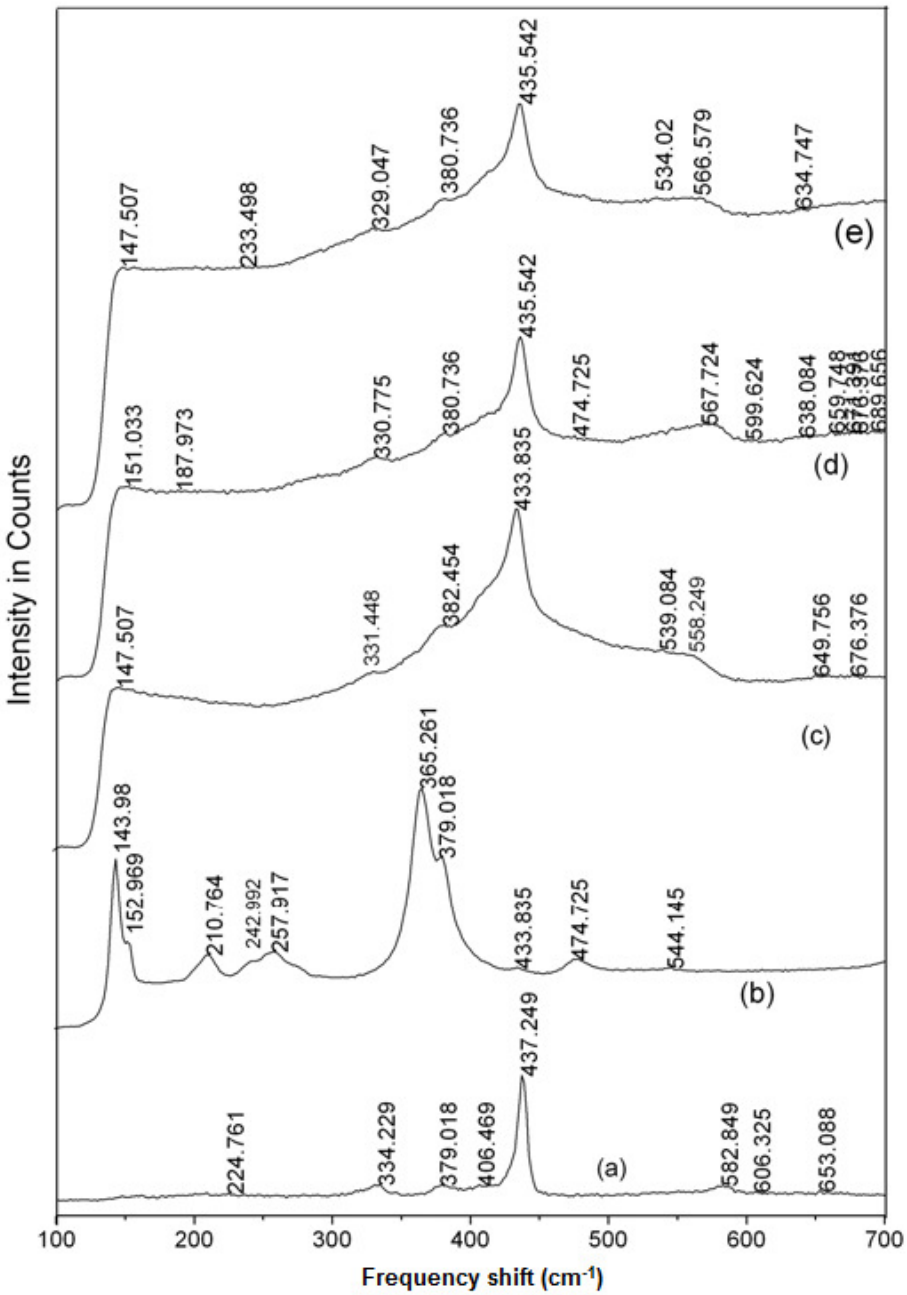

Figure 2. Off-resonant Raman spectra of arsenic-deposited films.
(a) Bulk powder, (b) Un-doped, (c) 2.5 at. wt. %, (d) 5.0 at. wt. %, (e) 7.5 at. wt. % aluminum doped.

In Sn-doped ZnO, the E_2 (high) phonon mode is the only dominating mode, whereas in Al-doped ZnO, the A_1(LO) mode is much less intense. In as-deposited films, vacancy point defects are supported by the presence of mixed modes of E_1(LO) and A_1(LO). Vacancies result in decreasing LO mode frequencies and a weakening of the long-range electrostatic force field. However, in the annealed thin films' Raman spectra, these modes are absent. This is in line with the theory that, during thermal annealing, point defects is eliminated from the lattice. When compared to annealed samples, it is discovered that all of the corresponding maxima in arsenic deposited layers are red shifted. This is consistent with the findings revealed about ZrO_2 nano particles by Liu et al. According to Liu et al. [13], the surface phonon-related Raman peak decreases and changes towards a lower wave number as particle size rises, whereas the other peaks change directions. This is consistent with what we observed in the ZnO system. According to some writers [14], the 2nd order Raman spectrum produced by the zone border phonons 2-TA, 2-E_2, and 2-LA phonons has extra modes at 208 cm^{-1}, 331 cm^{-1}, and 542 cm^{-1}, respectively. It is impossible to ignore the significance that lattice disorder's magnitude and stress-induced effects played in the development and alteration of the Raman peaks' width and intensity, though.

Table 1. Assignment of laser Raman bands in ZnO system

Sample description		Phonon modes assigned according to literature (cm^{-1})				Additional modes (cm^{-1}) observed
		E_2(low) [6]	A_1(T) [6]	E_2(High) [6]	Multiple phonon process [5, 14]	
ZnO pure powder (99.9999%)		---	379	437	334	225, 583(E_1LO)
Vacuum evaporated as-deposited films	ZnO	112	361	435	325	173, 206, 269, 470, 553
	ZnO: Al (5.0 at. wt %)	109	---	---	333, 671	551, 576
Vacuum evaporated annealed at 350°C for 2 hours in air	ZnO undoped	103	---	425	312, 542	162, 198, 258
	ZnO: Al (5.0 at wt %)	109	---	---	---	149
Dip Dried as – deposited films	ZnO	---	379	434	365	144, 153, 211, 243, 258, 475, 544
	2.5 at wt % Al doped ZnO	---	382	434	331	147, 539, 558(A1LO)
	5.0 at wt % Al doped ZnO	---	381	435	331	151, 475, 568(A1LO)
	7.5 at wt % Al doped ZnO	---	---	435	329	147, 233, 534, 566 (A_1LO)

Acknowledgements

The author would like to thank Dr. Manjeet Singh, Assistant Professor, G.C, Matanhail (Jhajjar) for many useful suggestions to carry out this research work.

References

[1] U. Ozgur, Y.I. Alivov, C. Liu, A. Teke, M.A. Reshchikov, S. Doğan, V. Avrutin, S.J. Cho, H. Morkoç, A comprehensive review on ZnO materials and devices, *J. App. Phys.* **98** (2005) 041301.

[2] H. Zhou, H. Alves, D.M. Hofmann, W. Kriegseis, B.K. Meyer, G. Kaczmarczyk, A. Hoffmann, Behind the weak excitonic emission of ZnO quantum dots: ZnO/Zn(OH)(2) core-shell structure, *Appl. Phys. Lett*. **80** (2002) 210-212.

[3] M. Rajalakshmi, A.K. Arora, B.S. Bendre, S. Mahamuni, Optical phonon confinement in zinc oxide nanoparticles, *J. Appl. Phys*. **87** (2000) 2445.

[4] A. Kaschner, U. Haboeck, M. Strassburg, M. Strassburg, G. Kaczmarczyk, A. Hoffmann, C. Thomsen, A. Zeuner, H.R. Alves, D.M. Hofmann, B.K. Meyer, Nitrogen-related local vibrational modes in ZnO:N, *Appl. Phys. Lett*. **80** (2002) 1909.

[5] C. Bundesmann, N. Ashkenov, M. Schubert, D. Spemann, T. Butz, E.M. Kaidashev, M. Lorenz, M. Grundmann, Raman scattering in ZnO thin films doped with Fe, Sb, Al, Ga, and Li, *Appl. Phys. Lett*. **83** (2003) 1974.

[6] N. Ashkenov, B.N. Mbenkum, C. Bundesmann, V. Riede, M. Lorenz, D. Spemann, E.M. Kaidashev, A. Kasic, M. Schubert, M. Grundmann, Infrared dielectric functions and phonon modes of high-quality ZnO films, *J. Appl. Phys*. **93** (2003) 126.

[7] X.H. Zhang, Y.C. Liu, X.H. Wang, S.J. Chen, G.R. Wang, J.Y. Zhang, Y.M. Lu, D.Z. Shen, X.W. Fan, Structural properties and photoluminescence of ZnO nanowalls prepared by two-step growth with oxygen-plasma-assisted molecular beam epitaxy, *J. Phys.: Condens. Matter* **17** (2005) 3035.

[8] J.F. Xu, W. Ji, X.B. Wang, H. Shu, Z.X. Shen, S.H. Tang, Temperature dependence of the Raman scattering spectra of Zn/ZnO nanoparticles, *J. Raman Spectr.* **29** (1998) 613-615.

[9] R. Loudon, The Raman effect in crystals, *Advan. Phys*. **13** (1964) 423-482.

[10] K.A. Alim, V.A. Fonoberov, M. Shamsa, A.A. Balandin, Micro-Raman investigation of optical phonons in ZnO nanocrystals, *J Appl. Phys*. **97** (2005) 124313.

[11] H. Ritcher, Z.P. Wang, L. Ley, The one phonon Raman spectrum in microcrystalline silicon, *Solid State Commun*. **39** (1981) 625-629.

[12] G. Abstreiter, E. Bauser, A. Fischer, Raman spectroscopy – A versatile tool for characterization of thin films and heterostructures of GaAs and $Al_xGa_{1-x}As$, *Appl. Phys*. **16** (1978) 345-352.

[13] F.X Liu, J.L. Yang, T.P. Zhao, Raman and Fourier-transform infrared photoacoustic spectra of granular ZrO_2, *Phys. Rev. B* **55** (1997) 8847.

[14] T.C. Damen, S.P.S. Porto, B. Tell, Raman effect in zinc oxide, *Phys. Rev*. **142** (1966) 570-574.